Journal of Sound and Vibration (2003) **259**(4), 779–796
doi:10.1006/jsvi.2002.5114, available online at http://www.idealibrary.com on IDEAL®

AN ACOUSTIC TRANSFORMER COMPOSED OF HORNS AND ITS APPLICATION

W. Moon and Y. G. Kim

Department of Mechanical Engineering, Pohang University of Science and Technology, San 31 *Hyojadong Namgu, Pohang Kyungbuk* 790-784*, South Korea. E-mail: wkmoon@postech.ac.kr*

(*Received* 26 *March* 2001, *and in final form* 19 *March* 2002)

A new acoustic transformer was developed by connecting three horns to improve radiation performance in the frequency region below 500 Hz. The proposed acoustic transformer was evaluated by numerical analysis using the commercial computer program SYSNOISE and by experiment. The acoustic transformer is composed of three horns, one of which was used in an inverted form. A design model was developed by use of Webster's horn equation and showed that the transformer can improve radiation efficiency. This was confirmed by numerical calculation using SYSNOISE. An acoustic projector was designed by use of the developed transformer and a piezoelectric unimorph-type actuator. The sound pressure measured at the mouth of the constructed acoustic projector was compared with the sound pressures evaluated at the same location by numerical calculation to investigate the differences between the numerical simulation model and the actual acoustic projector. Sound pressures generated by several acoustic radiators were calculated numerically and compared with the measured and calculated sound pressures of the developed acoustic projector to evaluate the effects of use of the proposed acoustic transformer. The comparative evaluation shows that the proposed acoustic transformer can provide up to a 10 dB gain over use of a horn in the narrow band low-frequency region from 100 to 200 Hz.

1. INTRODUCTION

The size of the radiation surface of a vibrating object is important for efficient acoustic radiation. Theoretically the load due to sound radiation reaches its maximum when the size of the radiation surface is almost equal to the wavelength of the sound generated. In real situations, it is nearly impossible to construct a sound generator with a radiation surface large enough to radiate low-frequency sounds efficiently. A horn has been used to improve the radiation efficiency of acoustic transducers by increasing radiation resistance and focusing the generated acoustic waves.

A horn is a type of waveguide with a variable cross-section area. In many acoustic devices, the role of the horn is to help acoustic waves to propagate from one region in a waveguide to a region with larger cross-sectional area with a little reflection as possible. The mouth of a horn, which has the larger cross-sectional area, is usually connected to an open acoustic medium such as air or seawater. For this reason a horn is sometimes called an acoustic transformer. The effects of a horn as an acoustic transformer are excellent. In general, an acoustic radiation device using a horn is known to have a radiation efficiency of up to 20%, while the radiation efficiency of a loudspeaker without a horn is from 0·1 to 2%. In the early 20th century the radiation amplification effects of horns were widely studied because it was the only way to amplify the acoustic waves directly generated by

0022-460X/02/$35.00

mechanical vibrations [1–4]. With the advent of electrical amplifiers and electromechanical loudspeakers the role of the horn has changed. The directional properties of a horn have been more frequently studied in recent years [3–5].

Horns are not used for hi-fidelity loudspeakers because they tend to distort low-frequency sound generated by the acoustic driver. Theoretical studies have been made to find a more rigorous wave equation for a horn in the belief that proper design of the horn cross-sectional area could eliminate the acoustic distortions generated by horns [5–7]. Geddes claimed that a new exact wave equation for wave propagation in a horn should be derived because Webster's horn equation is only approximate. He tried to derive a one-parameter wave equation using curvilinear co-ordinate systems. In response to Geddes's papers, Putland claimed that it is impossible to find an exact one-parameter wave equation in an arbitrary curvilinear co-ordinate system [8, 9]. It is shown in his paper that any one-parameter wave equation is in the form of Webster's horn equation and that the well-known wave equations such as spherical or plane wave equations are the only one-parameter wave equations that can be derived from the general linear wave equation [8].

In spite of the fact that a horn may not be a satisfactory acoustic transformer, no other device can replace its role as an acoustic transformer. In this paper, a waveguide composed of three horns is studied for use as an acoustic transformer for low-frequency acoustic projectors such a low-frequency SONAR. An direct generation method based on non-linear interaction of acoustic waves has been widely used to generate low-frequency sound for the low-frequency active SONAR system because the conventional method for sound generation cannot generate low-frequency sound with an acceptable efficiency [10, 11]. It is useful for the low-frequency active SONAR system to improve the radiation efficiency of low-frequency sound considerably.

It is well known that a horn can provide a good gain in radiation efficiency of low-frequency sound generation. However, it does not guarantee any advantage below a certain frequency, such as the cut-off frequency of exponential horns. In order to improve the characteristics of horns as acoustic transformers, a three-horn waveguide is studied here. The three-horn waveguide was made by combining two consecutive horns with an exponential horn at their throats. The expected advantage of this combination is an increase in acoustic radiation performance in the frequency region lower than the cut-off frequency of the inverse exponential horn, since the particle velocity can be amplified through the inverse horn.

In this paper, the properties of one type of the proposed three-horn waveguide are investigated theoretically and experimentally. By combining models for the three horns that comprise the waveguide, an analytic model based on Webster's horn equation for three-horn waveguide was developed. The derived model was used for designing and fabricating a real three-horn waveguide for experimental evaluation of its effects on the generation of low-frequency acoustic waves.

2. MODELLING OF AN ACOUSTIC TRANSFORMER

A three-horn acoustic transformer was designed by use of a formula that can be derived from Webster's horn equation. The procedure for developing the design model was composed of three parts: calculation of the transmission characteristics of an exponential horn of finite length; calculation of the transmission characteristics of a conical horn of finite length; and the combining of the transmission characteristic of two exponential horns—one that is used in the forward direction, the other in the backward direction—and a conical horn. The shape of the three-horn acoustic transformer is illustrated in Figure 1. This configuration is similar to the one presented by Keele [12].

The following three subsections describe the theoretical approach used to obtain the formula for calculating the acoustic characteristics of the three-horn acoustic transformer proposed in this paper. The approach is basically similar to the method to calculate transmission impedance of an exponential horn found in Beranek *et al.* [13–15]. The first two subsections are on the analytic methods for calculating the transmission characteristics of exponential and conical horns based on Webster's horn equation and the last subsection is on how to combine the results for use in the design of the transformer.

2.1. MODELLING OF EXPONENTIAL HORNS AND BACKWARD EXPONENTIAL HORNS

The analytic solution of Webster's horn equation for exponential horns is well known. The following is Webster's horn equation:

$$\frac{\partial^2 p}{\partial x^2} + \frac{\partial}{\partial x}(\ln S)\frac{\partial p}{\partial x} - \frac{1}{c^2}\frac{\partial^2 p}{\partial t^2} = 0, \tag{1}$$

where p, c, and S are acoustic pressure, sound propagation speed and the cross-sectional area of the horn respectively.

The cross-sectional area of exponential horns illustrated in Figure 2 can be expressed by $S = S_0 e^{mx}$ where S_0 is the cross-sectional area at the throat and m represents the flare constant of exponential horns. It is well known that exponential horns have a cut-off frequency, f_c. In the frequency region under the cut-off frequency waves will not propagate theoretically in the forward direction. The cut-off frequency is related to the propagation speed c and the flare constant $m = 4\pi f_c/c$ [16, 17]. In the case of exponential horns, Webster's horn equation reduces to the following simple solvable form:

$$\frac{\partial^2 p}{\partial x^2} + m\frac{\partial p}{\partial x} - \frac{1}{c^2}\frac{\partial^2 p}{\partial t^2} = 0. \tag{2}$$

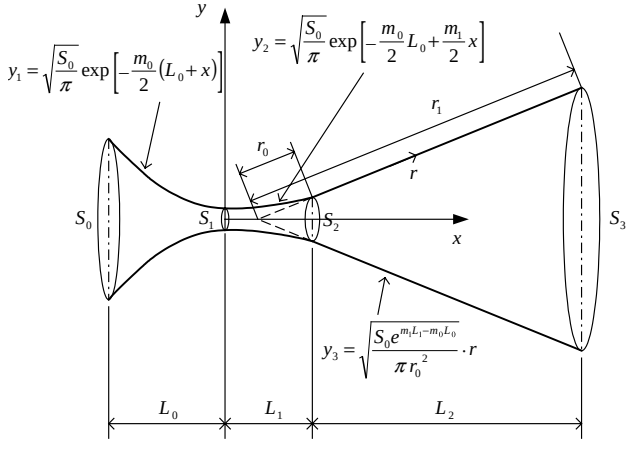

$$x - x_0 = \frac{r}{r_0}\sqrt{r_0^2 - S_2/\pi}, \quad x_0 = L_1 - \sqrt{r_0^2 - S_2/\pi}, \quad r_1 = r_0\sqrt{\frac{S_3}{S_2}},$$

$$S_2 = S_0 e^{-m_0 L_0 + m_1 L_1}, \quad L_2 = (r_1 - r_0)\sqrt{1 - \frac{S_2}{m r_0^2}}$$

Figure 1. A three-horn acoustic transformer.

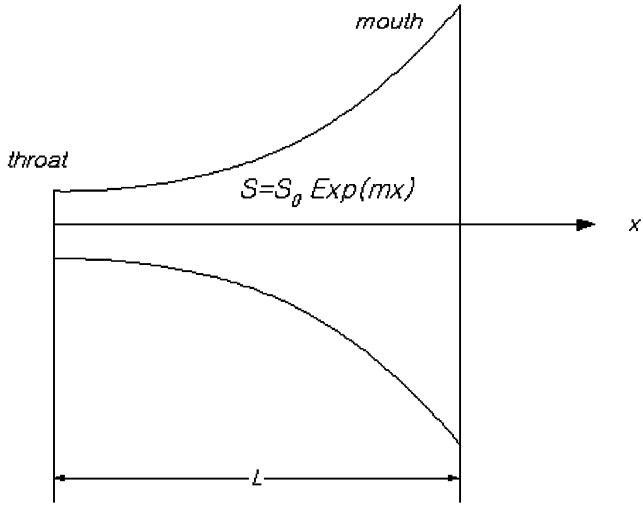

Figure 2. An exponential horn.

The solution of Equation (2) can be expressed as follows:

$$p = A\mathrm{e}^{-\mathrm{j}(\beta-\mathrm{j}\alpha)x} + B\mathrm{e}^{-\mathrm{j}(-\beta-\mathrm{j}\alpha)x}, \tag{3}$$

where

$$\pm\beta + \mathrm{j}\alpha = \begin{cases} k\mathrm{e}^{\mathrm{j}\theta} \\ -k\mathrm{e}^{-\mathrm{j}\theta} \end{cases} = \pm\sqrt{k^2 - \frac{m^2}{4}} + \mathrm{j}\frac{m}{2},$$

$$\alpha = \frac{m}{2}, \quad \beta = \sqrt{k^2 - \frac{m^2}{4}}, \quad \theta = \tan^{-1}\left(\frac{m}{2\beta}\right).$$

By use of Equation (3) and the approximate momentum equation in linear acoustics, the particle velocity can be expressed as follows:

$$u = \frac{\mathrm{e}^{-\alpha x}}{\rho c}[A\mathrm{e}^{-\mathrm{j}(\theta+\beta x)} - B\mathrm{e}^{\mathrm{j}(\theta+\beta x)}]. \tag{4}$$

Now the transmission matrix that represents the transmission characteristics of a horn of finite length can be calculated using Equation (4). The particle velocities and the acoustic pressures at the throat and mouth are related by a matrix as follows:

$$\begin{bmatrix} p_m \\ u_m \end{bmatrix} = \begin{bmatrix} \mathrm{e}^{\alpha L}\dfrac{\cos(\theta+\beta L)}{\cos\theta} & \mathrm{j}\rho c\mathrm{e}^{\alpha L}\dfrac{\sin\beta L}{\cos\theta} \\ \dfrac{\mathrm{j}}{\rho c}\mathrm{e}^{\alpha L}\dfrac{\sin\beta L}{\cos\theta} & \mathrm{e}^{\alpha L}\dfrac{\cos(\theta-\beta L)}{\cos\theta} \end{bmatrix} \begin{bmatrix} p_t \\ u_t \end{bmatrix}, \tag{5}$$

where the subscripts $(\,)_t$ and $(\,)_m$ represent pressure and velocity at the throat and mouth respectively. Equation (5) can be obtained by substituting the following expressions into equations (3) and (4):

$$A = \mathrm{e}^{\alpha L}\frac{-(p_m/\rho c)\mathrm{e}^{\mathrm{j}(\theta+\beta L)} - u_m\mathrm{e}^{\mathrm{j}\beta L}}{-(1/\rho c)[\mathrm{e}^{\mathrm{j}\theta} + \mathrm{e}^{-\mathrm{j}\theta}]}, \quad B = \mathrm{e}^{\alpha L}\frac{-(p_m/\rho c)\mathrm{e}^{-\mathrm{j}(\theta+\beta L)} + u_m\mathrm{e}^{\mathrm{j}\beta L}}{-(1/\rho c)[\mathrm{e}^{\mathrm{j}\theta} + \mathrm{e}^{-\mathrm{j}\theta}]}. \tag{6}$$

Equation (5) can be used for calculating the transmission characteristics of a backward exponential horn of finite length. The transmission matrix may be the inverse matrix of the transmission matrix shown in Equation (5).

2.2. MODELLING OF CONICAL HORNS

The governing equation of a conical horn can be derived through two paths: Webster's horn equation and the spherical wave equation. As mention in the introduction it shows that the governing equation of a conical horn is one of the existing one-parameter wave equations. The equation for conical horns is exact if the propagating wave through the horn is a spherical wave. In Webster's horn equation, a plane wave is assumed to be valid. The difference between the theories for a conical horn based on the spherical wave equation and Webster's horn equation becomes obvious at the throat. In the case of exponential horns, the assumptions of Webster's horn equation are acceptable at the throat only if the flare constant is sufficiently small. For a spherical wave propagating through a conical horn, the assumptions cannot be valid at its throat.

Now, if the cross-sectional area of a conical horn is set to be $S = S_0 r^2$ as shown in Figure 3, the exact one-parameter wave equation based on spherical waves may be expressed as follows:

$$\frac{\partial^2 p}{\partial r^2} + \frac{2\partial p}{r\,\partial r} - \frac{1}{c^2}\frac{\partial^2 p}{\partial t^2} = 0, \tag{7}$$

where r is the component of a location in the radial direction of a spherical co-ordinate system.

The velocity potential function φ of spherical waves is well known:

$$\varphi = \frac{A}{r} e^{\,j(\omega t - k(r - r_0))} + \frac{B}{r} e^{\,j(\omega t + k(r - r_0))} \tag{8}$$

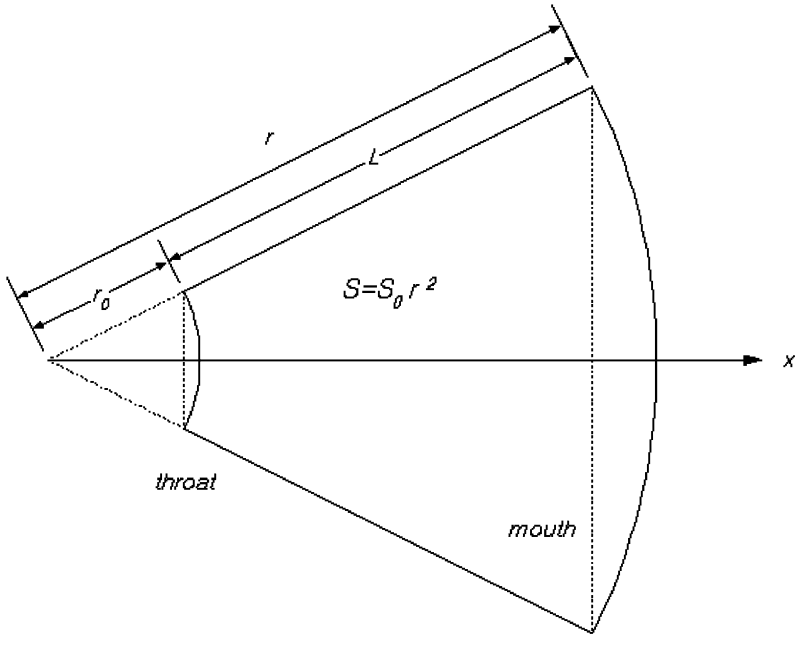

Figure 3. Conical horn.

By use of the relations $p = -p\partial\varphi/\partial t$ and $u = \nabla\varphi$, the following relations similar to those found in reference [18] between pressures and velocities at the mouth and throat can be obtained as before:

$$\begin{bmatrix} p_t \\ u_t \end{bmatrix} = \begin{bmatrix} \left(\frac{r_1}{r_0}\right)\cos kL - \left(\frac{1}{kr_0}\right)\sin kL & \mathrm{j}\rho c\left(\frac{r_1}{r_0}\right)\sin kL \\ \bar{c} & \left(\frac{r_1}{r_0}\right)\left[\cos kL + \left(\frac{1}{kr_0}\right)\sin kL\right] \end{bmatrix} \begin{bmatrix} p_m \\ u_m \end{bmatrix}, \quad (9)$$

where

$$\bar{c} = \frac{\mathrm{j}}{\rho c}\left[\left(\frac{r_1}{r_0} + \frac{1}{(kr_0)^2}\right)\sin kL - \frac{L}{r_0}\frac{1}{kr_0}\cos kL\right]$$

and r_1 is the radius of the outlet cross-section.

2.3. ANALYSIS OF THE EACH PART

Since the three-horn acoustic transformer is composed of a backward and forward exponential horn and a conical horn, the transmission matrix for the three-horn acoustic transformer may be calculated using the transmission matrices obtained in the previous section for the individual horns. After calculating the pressure and particle velocity, the impedance is calculated at the location of the transducer by use of the transmission matrices derived in the previous section. The radiation impedances of the conical, and the backward and the forward exponential horns are given as Z_{con}, Z_{b_exp}, and Z_{f_exp}, respectively, in the following:

$$Z_{con} = S_2\frac{\bar{a}_2 Z_3 + \bar{b}_2 S_3}{\bar{c}_2 Z_3 + \bar{d}_2 S_3}, \quad Z_{b\_exp} = S_0\frac{\bar{a}_0 Z_1 + \bar{b}_0 S_1}{\bar{c}_0 Z_1 + \bar{d}_0 S_1}, \quad Z_{f\_exp} = S_1\frac{\bar{a}_1 Z_2 + \bar{b}_1 S_2}{\bar{c}_1 Z_2 + \bar{d}_1 S_2}, \quad (10)$$

TABLE 1

Formula for the coefficients in the transmission matrices

Back exponential horn	Exponential horn	Conical horn
$\bar{a}_0 = \mathrm{e}^{-\alpha_0 L_0}\frac{\cos(\theta_0 - \beta_0 L_0)}{\cos\theta_0}$	$\bar{a}_1 = \mathrm{e}^{\alpha_1 L_1}\frac{\cos(\theta_1 + \beta_1 L_1)}{\cos\theta_1}$	$\bar{a}_2 = \left(\frac{r_1}{r_0}\right)\cos kL_2 - \left(\frac{1}{kr_0}\right)\sin kL_2$
$\bar{b}_0 = \mathrm{e}^{-\alpha_0 L_0}\mathrm{j}\rho c\frac{\sin\beta_0 L_0}{\cos\theta_0}$	$\bar{b}_1 = \mathrm{e}^{\alpha_1 L_1}\mathrm{j}\rho c\frac{\sin\beta_1 L_1}{\cos\theta_1}$	$\bar{b}_2 = \left(\frac{r_1}{r_0}\right)\mathrm{j}\rho c\sin kL_2$
$\bar{c}_0 = \mathrm{e}^{-\alpha_0 L_0}\frac{\mathrm{j}}{\rho c}\frac{\sin\beta_0 L_0}{\cos\theta_0}$	$\bar{c}_1 = \mathrm{e}^{\alpha_1 L_1}\frac{\mathrm{j}}{\rho c}\frac{\sin\beta_1 L_1}{\cos\theta_1}$	$\bar{c}_2 = \frac{\mathrm{j}}{\rho c}\left[\left(\frac{r_1}{r_0} + \left(\frac{1}{kr_0}\right)^2\right)\sin kL_2 - \left(\frac{L_2}{r_0}\right)\left(\frac{1}{kr_0}\right)\cos kL_2\right]$
$\bar{d}_0 = \mathrm{e}^{-\alpha_0 L_0}\frac{\cos(\theta_0 + \beta_0 L_0)}{\cos\theta_0}$	$\bar{d}_1 = \mathrm{e}^{\alpha_1 L_1}\frac{\cos(\theta_1 - \beta_1 L_1)}{\cos\theta_1}$	$\bar{d}_2 = \left(\frac{r_1}{r_0}\right)\left[\cos kL_2 + \left(\frac{1}{kr_0}\right)\sin kL_2\right]$

where Z_1, Z_2, Z_3, S_1, S_2 and S_3 are the mechanical impedances at and the cross-section area of the outlets of the conical, and the backward and forward exponential horns respectively. The coefficients in equation (10) are given in Table 1. Using these expressions, the radiation impedance of the three-horn acoustic transformer can be calculated as follows:

$$Z_{trans} = S_0 \frac{(\bar{a}_0\bar{a}_1\bar{a}_2 + \bar{a}_0\bar{b}_1\bar{c}_2 + \bar{b}_0\bar{c}_1\bar{a}_2 + \bar{b}_0\bar{d}_1\bar{c}_2)Z_3 + (\bar{a}_0\bar{a}_1\bar{b}_2 + \bar{a}_0\bar{b}_1\bar{d}_2 + \bar{b}_0\bar{c}_1\bar{b}_2 + \bar{b}_0\bar{d}_1\bar{d}_2)S_3}{(\bar{c}_0\bar{a}_1\bar{a}_2 + \bar{c}_0\bar{b}_1\bar{c}_2 + \bar{d}_0\bar{c}_1\bar{a}_2 + \bar{d}_0\bar{d}_1\bar{c}_2)Z_3 + (\bar{c}_0\bar{a}_1\bar{b}_2 + \bar{c}_0\bar{b}_1\bar{d}_2 + \bar{d}_0\bar{c}_1\bar{b}_2 + \bar{d}_0\bar{d}_1\bar{d}_2)S_3}. \tag{11}$$

In this expression the coefficients are also given in Table 1 and Z_3 is the impedance at the outlet whose cross-section area in S_3 as shown in Figure 1.

Figure 4 shows the real dimensions of the fabricated three-horn acoustic transformer. The computer program Mathematica was used for numerical calculations. In order to calculate the impedance at the inlet (where sound in generated, or an acoustic transducer is located), the impedance at the outlet (where sound is radiated to air) needs to be known. The radiation impedance of a circular piston with infinite baffle is selected as the

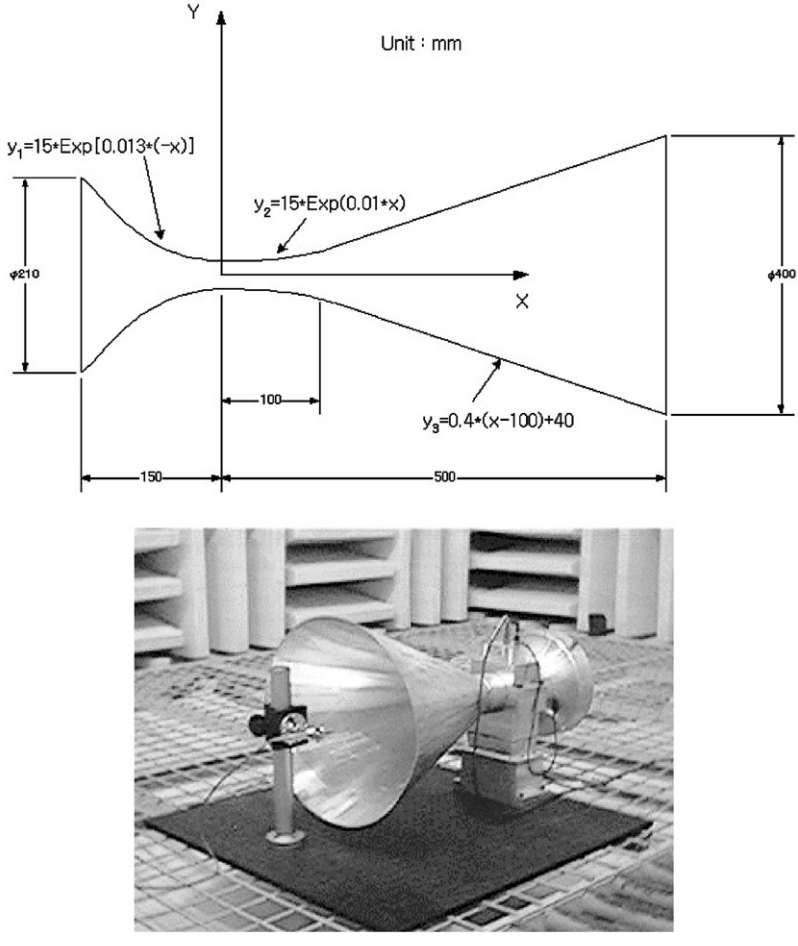

Figure 4. Overview of the new acoustic transformer.

impedance at the outlet. This selection may make the calculated resistance larger than its actual value. In numerical calculations only the resistance, the real part of the impedance, is calculated because it is the important factor for the radiation efficiency.

We first consider the radiation resistance of each part. Figure 5 shows the frequency response of radiation resistance of a backward exponential horn. The thing of interest in this figure is that there are many peaks in the graph. Those peaks are much higher than the peaks for the forward exponential horn illustrated in Figure 6. Since the outlet area (throat) is much smaller than the inlet area (mouth) in the backward exponential horn, this horn acts more like a cavity than the forward exponential horn. Hence, its peaks are higher. The most interesting fact is that there exists a peak below the cut-off frequency. In Figure 5, an abrupt change in the curve can be seen at around 700 Hz. It is caused by the cut-off frequency. In the region between 200 and 400 Hz, one peak is found which may imply that radiation efficiency could be improved if the backward exponential horn is properly used. As seen in Figure 6, this effect is not evident in the forward exponential horn.

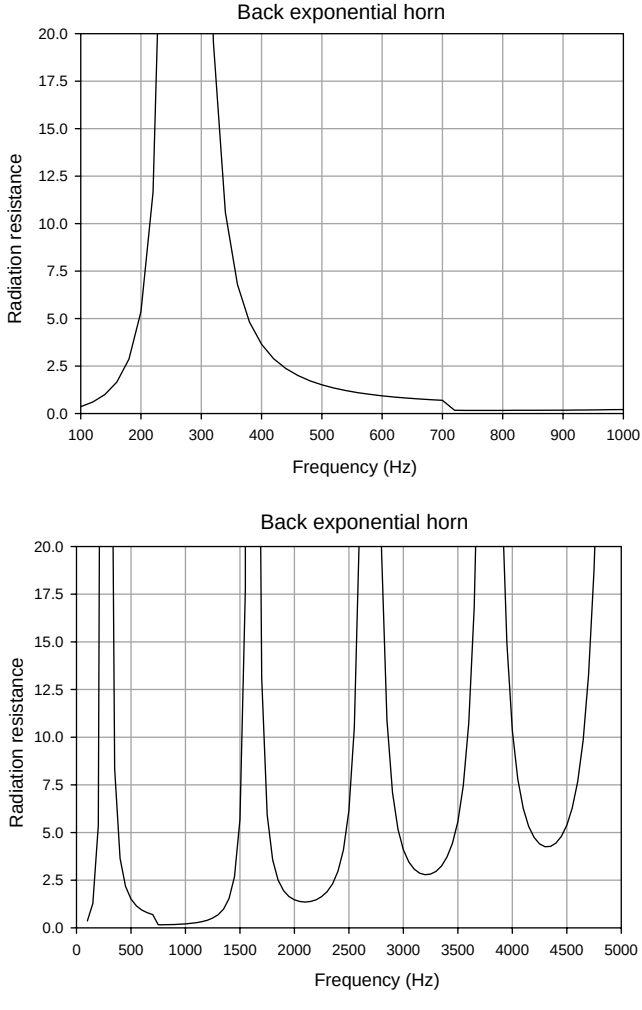

Figure 5. Radiation resistance of the back exponential horn.

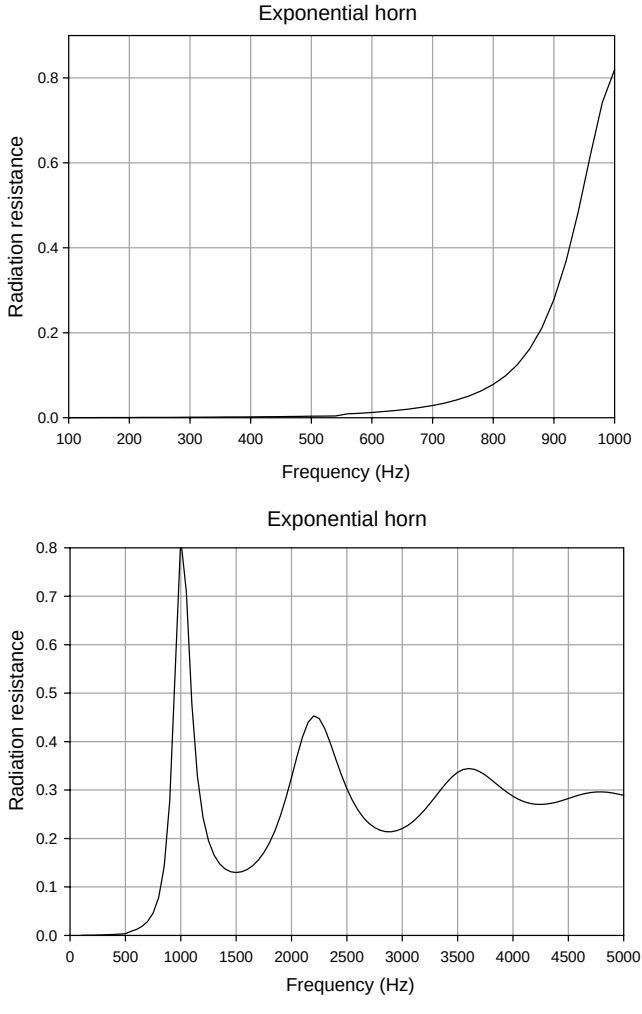

Figure 6. Radiation resistance of the exponential horn.

The cut-off frequency of the forward exponential horn, whose resistance is shown in Figure 6, is 500 Hz. Although there are many peaks that are due to its finite length, the overall shape of the curve represents the radiation resistance of an exponential horn. Note that the radiation effects are negligibly small in the frequency region below the cut-off frequency of 500 Hz.

The conical horn considered is quite a large one; hence, its radiation is larger than those of the exponential horns. The impedance curve is also smooth. These characteristics are easily observed in Figure 7. There are two peaks in the frequency region below 700 Hz. However, it is obvious in Figure 7 that their values are much smaller than the impedance values in saturation.

Now we consider the radiation resistance of the three-horn acoustic transformer. In Figure 8 its radiation resistance is shown to have a very large peak below 300 Hz with a value much larger than that of any other peak. This is a very interesting result because it suggests that the three-horn acoustic transformer can be more efficient for the generation of low-frequency sounds than a single horn that has the same inlet and outlet cross-

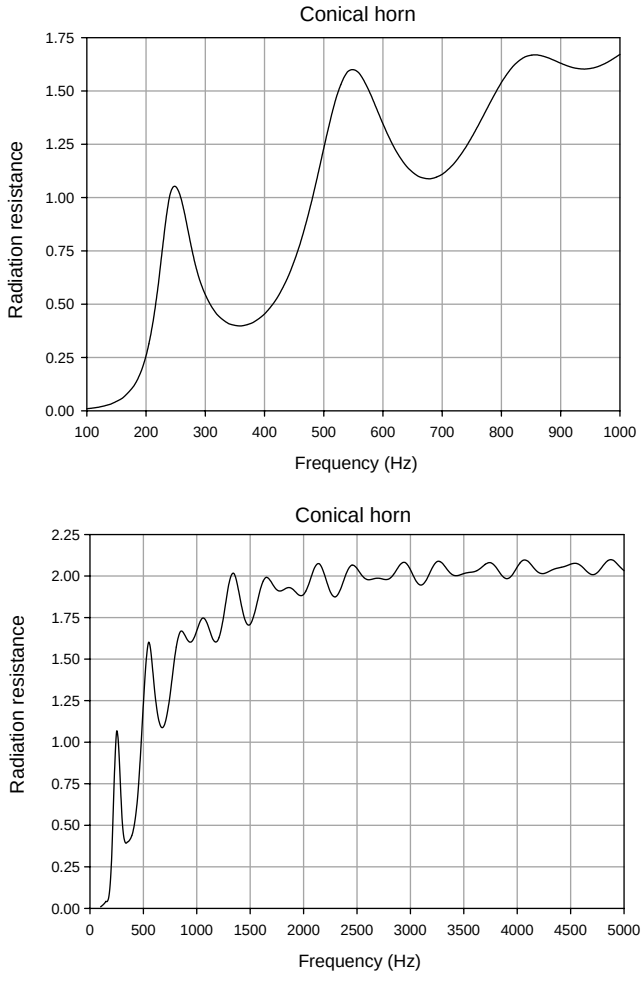

Figure 7. Radiation resistance of the conical horn.

sectional area as the transformer. This low-frequency peak can, of course, be expected since a backward exponential horn displays a peak in the low-frequency region (Figure 5). As mentioned above, horns were used for improving radiation efficiency at the beginning of the era of acoustic loudspeakers, and even today horns are used for this purpose when sound quality is not critically important and loudness is necessary. Since the value of the cut-off frequency depends on the flare constant, the flare constant should be small to generate sounds of low-frequency such as 100 Hz. However, a horn with a small flare constant should be very long in order to have an opening large enough to considerably improve radiation efficiency. The three-horn acoustic transformer considered here could be very useful since its total length required for improving radiation efficiency is smaller than that of a single horn.

Besides the peaks in the frequency region below the cut-off frequencies of the exponential horns used, other interesting characteristics of the three-horn acoustic transformer can be observed in Figure 8. First, there exist discontinuities around the cut-off frequencies of the exponential horns—a backward one and a forward one. Second, the

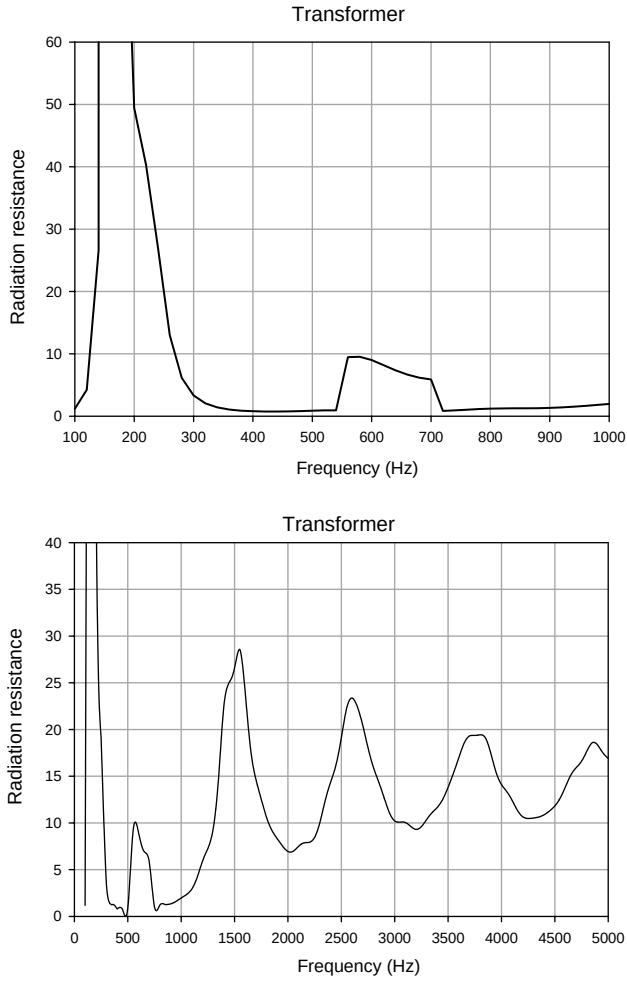

Figure 8. Radiation resistance of the acoustic transformer.

frequency of the peak (about 170 Hz) is not equal to the frequencies of the peaks if the backward and the forward exponential horns, or the conical horn, are considered separately (Figures 5, 6 and 7). Third, the frequency response curve is not smooth. Even though the peak-to-peak amplitude decreases with frequency, it does not seem to be adequate to be used for hi-fidelity loudspeakers.

From the considerations above, it is concluded that the three-horn acoustic transformer does not seem to have better frequency response characteristics for hi-fidelity loudspeaker but that it may be able to generate narrowband low-frequency sound more efficiently. This property may be very useful for applications such as low-frequency SONAR. The radiation improving effects should be confirmed by numerical analysis of systems closer to the real situations. In the following sections, we describe the numerical simulations performed using the commercial computer program SYSNOISE. Since the effects can be simulated by the numerical calculations, a three-horn acoustic transformer is constructed and examined by generating sounds using a plate that is excited by a piezoelectric unimorph. The results are described in the following section.

3. EXPERIMENT & SIMULATION

3.1. EXPERIMENT AND SIMULATION SET-UP

A sound generator was constructed using a three-horn acoustic transformer as illustrated in Figure 4. A vibrating circular plate, shown in Figure 9, was used as a radiating surface. A piezoelectric rectangular thin plate was attached at the center of the circular plate, in consideration of the conclusions by Clark *et al.* [19,20]. With a size of 20 mm wide, 20 mm long and 0·5 mm thick. The whole structure was made of aluminum and the material constants of the PZT plate are listed in Table 2. The PZT plated used is a product called C-8 from FUJI Ceramics Inc. in Japan. An adhesive (ALKA-SQ102) was used to combine the PZT and aluminum plates and its thickness was less than 0·1 mm. In the model for the aluminum and the PZT plates, the thickness of adhesive was ignored.

The three-horn transformer illustrated in Figure 4 was connected with the circular vibrating plate by bolts. The three horns were made of aluminum and welded at their joints. The sizes and shapes of the three horns were identical to those of the three horns described and investigated in section 2.

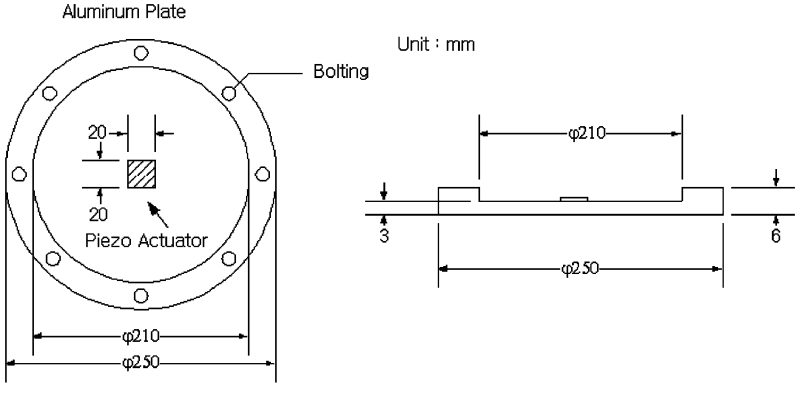

Figure 9. Aluminum plate and piezoelectric ceramic actuator.

TABLE 2

Mechanical properties of the piezoelectric ceramic PZT used in the experiment

Property	Symbol	Value
Young's modulus	E_{11}	59×10^9 Pa
Young's modulus	E_{33}	52×10^9 Pa
Young's modulus	E_{55}	21×10^9 Pa
Piezoelectric charge constants	d_{31}	-260×10^{-12} C/N
Piezoelectric charge constants	d_{33}	540×10^{-12} C/N
Piezoelectric charge constants	d_{15}	750×10^{-12} C/N
Piezoelectric voltage constants	g_{31}	$-8{\cdot}7 \times 10^{-3}$ m^2/C
Piezoelectric voltage constants	g_{33}	18×10^{-3} m^2/C
Piezoelectric voltage constants	g_{15}	$27{\cdot}5 \times 10^{-3}$ m^2/C
Relative dielectric constants	$\varepsilon_{11}/\varepsilon_0$	3100
Relative dielectric constants	$\varepsilon_{33}/\varepsilon_0$	3400

In numerical simulations, the commercial program SYSNOISE was used. The structural properties of the circular plate were investigated using the structure analysis module of SYSNOISE and its first natural frequency was found to be 528 Hz. As expected, the mode shape of the first mode was not planar. Hence, the structure–acoustic interactions were considered using the module for structure–acoustic interactions in SYSNOISE.

The conditions for simulations and experiments were of two types: a constant-velocity condition and a constant-voltage condition. The constant-velocity condition implies that the velocity of the vibrating circular plate is maintained constant. Since the velocity distribution on the plate is not uniform the maximum velocity at the center was selected as a representative velocity. In simulations, the velocity distribution of the first mode was assumed. The frequency responses of velocities at several points were measured using a laser interferometer (PolyTec OFV-3001, OFV-511); the experimental set-up for the measurement is shown in Figure 10. The measured frequency response curves at several points are shown in Figure 11. As expected, the velocity distribution is not uniform and displays a maximum at the center in the frequency regions from 0 to 520 Hz and above 800 Hz.

As can be seen in Figure 11, the velocity was not constant with frequency even though the applied voltage at the piezoelectric actuator was constant. In experiments, however, a constant-velocity condition is hard to realize because the velocity at any location varies

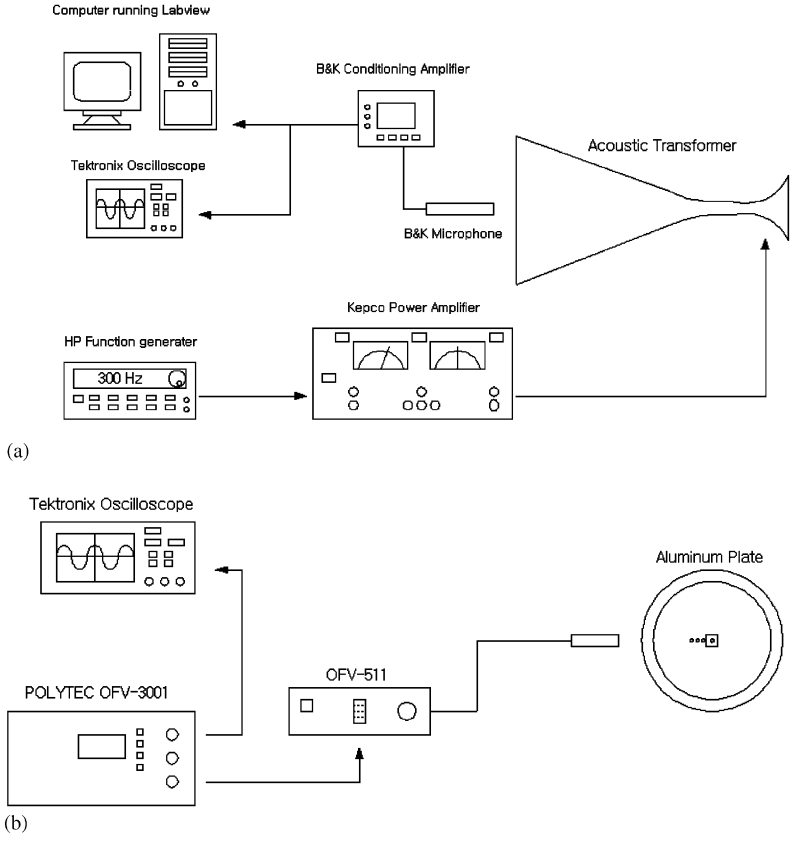

Figure 10. Experimental set-ups (a) for measurements of the sound pressure at the axis in front of the opening, and (b) for measurement of the velocity at the center of the vibrating sound-radiating plate.

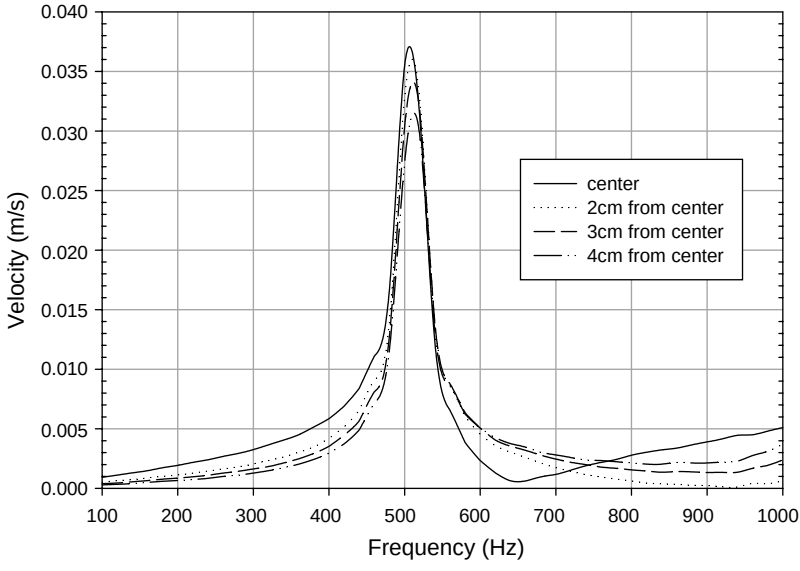

Figure 11. Frequency–velocity curve at several points.

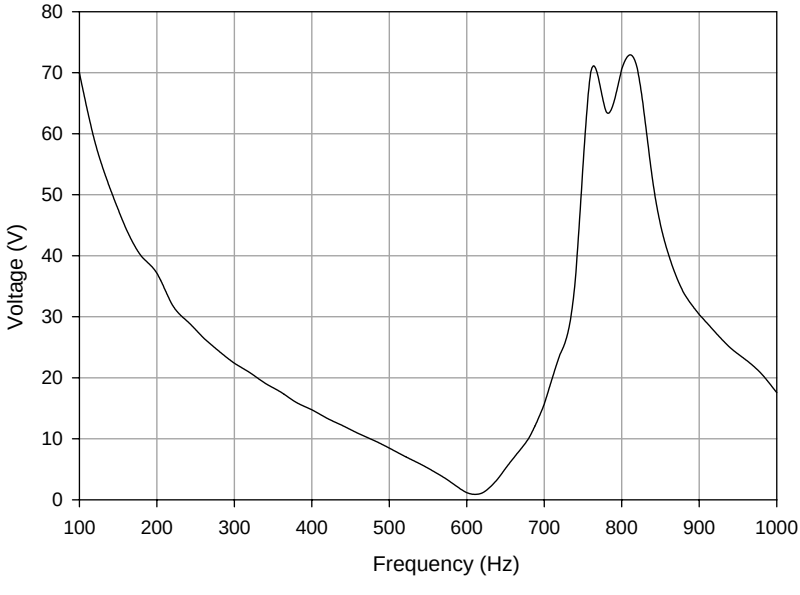

Figure 12. Frequency–voltage relation for constant velocity condition.

considerably, as illustrated in Figure 11. Figure 12 shows the voltage variation with frequency while the measured velocity at the center is maintained to be as constant as possible. It is difficult to maintain a constant velocity since the voltages around the resonance frequency is very small compared with the voltages at 0 Hz and 700–800 Hz. The constant-voltage condition is more natural and easier to maintain in experiments. For acoustic considerations, the constant-velocity condition is more convenient.

In order to experimentally investigate the effects of the three-horn acoustic transformer, the acoustic pressure at the center of the outlet of the three-horn transformer was measured using a half-inch microphone (B&K 4190) inside an anechoic room while electric voltage was applied to the piezoelectric actuator at various frequencies. The measured pressure was transferred to a computer through a data acquisition H/W (NI PCI-MIO-16XE-10) and S/W (LabVIEW). The pressure measurement was performed from 100 Hz to 1 kHz in 20 Hz increments. For the constant-voltage condition the applied voltage was kept at 60 V. For the constant-velocity condition the pressure was measured while the velocity at the center of circular plate was controlled to be around 0·00228 m/s. In reality, the voltage was controlled by hand at a fixed frequency so that the velocity was the given value and this procedure was iterated at a higher frequency.

The pressure at the center of the outlet of the three-horn acoustic transformer was calculated using SYSNOISE at the same frequencies used for the experimental measurements. The calculation results are quite different from the results obtained by the analytic model derived in section 2. They are much closer to those from experiments. The frequency response curves are shown as graphs in Figures 13 and 14. The comparisons and characteristics are discussed in the next section.

3.2. RESULTS AND DISCUSSIONS

The constant-velocity condition is adequate to investigate the acoustic characteristic of the three-horn acoustic transformer since the output acoustic pressure amplitudes in this condition are directly related with the radiation efficiency. In Figure 13 the frequency characteristics are shown for the acoustic pressure amplitudes generated using the three-horn acoustic transformer. Several other curves are found in Figures 13 and 14. The solid line represents the measured frequency characteristics and the dotted line does the numerical simulation results by SYSNOISE. The dashed line shows the frequency characteristics calculated by SYSNOISE for the acoustic pressure amplitude generated

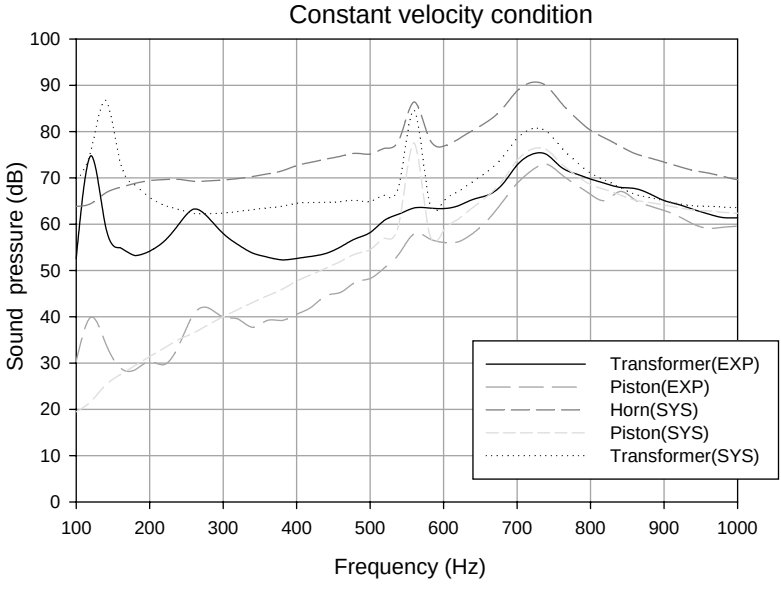

Figure 13. Acoustic pressure at the mouth in the constant velocity condition.

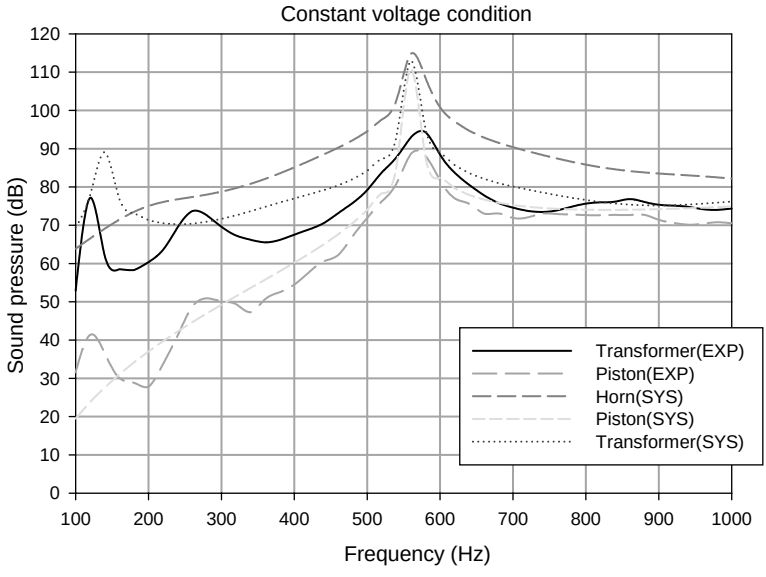

Figure 14. Acoustic pressure at the mouth in the constant voltage condition.

using a single exponential horn whose throat and mouth are identical to the inlet and outlet of the three-horn acoustic transformer respectively. The gray lines are the calculated and measured frequency characteristic curves of the acoustic pressure amplitudes using a bare vibrating plate.

First of all, if the solid line is observed carefully, it is easily found that there are four peaks and that the peak at lowest frequency is located at around 120 Hz. It is recalled that there is a big peak at approximately the same frequency in the frequency characteristic curve obtained by the analytic model in section 2 (Figure 8). As can be seen in Figure 8, the peak lies between 100 and 200 Hz. The dotted line obtained using SYSNOISE has a peak located closer to the frequency at which it is located in Figure 8. This implies that numerical simulations and experiments confirm the effects on acoustic radiation efficiency predicted in section 2. When the dotted line is compared with dashed line in the frequency region below 200 Hz, the calculated pressure generated using the three-horn acoustic transformer is larger than the calculated pressure generated using one exponential horn. Although the experiments provide smaller pressure values (the solid line) than the calculations do (the dotted line) for an identical case, in Figure 13 it can be seen that the solid curve from experiment is still higher in the narrow frequency region from 110 to 140 Hz than the dashed one from the numerical calculations. This implies that if a sound is generated using the three-horn acoustic transformer, its acoustic pressure is up to 20 dB larger in the narrowband frequency region from 100 to 180 Hz than that using one exponential horn. Since the curves in Figure 13 represent the results from numerical calculations or experimental measurements under the condition that the velocity amplitude of the radiation surface is maintained constant, the larger output acoustic pressure implies the more efficient sound generation. in other words, since the acoustic radiation loading increases with use of the three-horn acoustic transformer, the radiation power efficiency increases with it.

However, except the frequency region from 110 to 140 Hz, the pressure amplitudes using the three-horn acoustic transformer was up to 10 dB smaller than that using one

exponential horn. Although improvement in radiation efficiency is limited to narrowband frequency region, it is inspiring that the narrowband lies in the low-frequency region below 200 Hz. The narrowband region may be controlled by the geometry of the transformer. It is important that the three-horn acoustic transformer is more effective in the low-frequency region, because it is difficult to increase the radiation efficiency for low-frequency sounds in general. Till now horns are the most effective devices that improve radiation efficiency acoustically. Therefore, the three-horn acoustic transformer may be useful as a low-frequency sound generator such as a low-frequency SONAR projector. As mentioned earlier, the widely used indirect method can generate low-frequency sounds at most in "second order" magnitudes because it uses the non-linear interaction between two high frequency sounds [11]. Therefore, its power efficiency is not as large as the low-frequency sound generation using the developed acoustic transformer at least in the narrow frequency band where the acoustic transformer shows a large radiation resistance. But the acoustic transformer can make the sound emitting system bulkier, hence, it may cause a problem in the case that the size should be compact.

In the frequency region above the first resonance frequency (about 500 Hz) of the radiating plate, the curves from the numerical calculations using SYSNOISE may be different from the one shown in Figure 13 because the mode shape of the second mode is different from that of the first. Considering this effect, comparisons between the solid and the dotted curves in Figure 13 may be meaningless in this frequency region.

In Figure 14, the frequency response curves obtained from experiments and numerical calculations are shown the under the constant-voltage condition. The overall characteristics are not much different from those for the constant-velocity condition except for the effects of resonance of the radiating plate at around 550 Hz. The frequencies of the peaks due to resonance of the radiating plate shown in Figures 13 and 14 are somewhat different from the one found in Figure 11. It is explained by the fact that the tension was not the same for the bolts joining the plate and the transformer in those cases. It was found that the resonance frequency could vary from 500 to 580 Hz, depending on the bolt tension.

The frequency response curves in Figure 14 are smoother than those in the constant-velocity condition. It is believed that the fluctuations of the solid line from 500 to 900 Hz in Figure 13 may be caused by inaccuracy in the velocity control. It is interesting that the solid line in Figure 14 is flatter than the dashed line. This suggests that the sound generator using a three-horn acoustic transformer may be better in sound quality than a horn if the radiating plate is driven by a voltage source.

4. CONCLUSION AND RECOMMENDATIONS

In this paper the acoustic characteristics of a three-horn acoustic transformer are investigated. The three-horn acoustic transformer is constructed by connecting one backward exponential horn, one forward exponential horn and a conical horn. It is observed through calculations using an analytic model, numerical simulations using the commercial program SYSNOISE, and experiments, that the acoustic transformer can improve acoustic radiation efficiency in a narrowband frequency region. It is inspiring that the narrowband lies in the low-frequency region where horns are not very effective. Hence, it may be useful for devices such as low-frequency SONAR projectors.

The effects of the combination of various horns can be observed by studying the characteristics of the three-horn acoustic transformer numerically and experimentally. However, the physical parameters should be found to determine the bandwidth and center frequency of the frequency region where the transformer increases radiation efficiency. In

addition, whether the transformer can be successfully applied to low-frequency SONAR projectors is still to be investigated because it can make the system bulkier. These issues will be considered in our future work.

ACKNOWLEDGMENTS

The authors wish to thank Dr. J. Lee in Ulsan University for his help with the experiments. This work is supported by the Pohang University of Science and Technology.

REFERENCES

1. S. Ballantine 1927 *Journal of Franklin Institute* 85–103. On the propagation of sound in the general bessel horn of infinite length.
2. H. F. Olsen 1957 *Acoustical Engineering*, 100–115. New York: Van Nostrand.
3. J. E. Freehafer 1940 *Journal of the Acoustical Society of America* **11**, 467–476. An acoustical impedance of an infinite hyperbolic horn.
4. J. Hilliard 1976 *Journal of the Acoustical Society of America* **59**, 1–8. Historical review of horns used for audience type sound reproduction.
5. E. R. Geddes 1989 *Journal of the Audio Engineering Society* **37**, 554–569. Acoustic waveguide theory.
6. E. R. Geddes 1993 *Journal of the Audio Engineering Society* **41**, 452–461. Acoustic waveguide theory revisited.
7. E. R. Geddes 1986 *Journal of the Audio Engineering Society* (*Engineering Report*) **34**, 464–478. Source radiation characteristics.
8. G. R. Putland 1993 *Journal of the Audio Engineering Society* **41**, 435–451. Every one-parameter acoustic field obeys Webster's horn equation.
9. G. R. Putland and E. R. Geddes 1991 *Journal of the Audio Engineering Society* (Letters on the Editor) **39**, 469–472. Comments on 'Acoustic Waveguide Theory'.
10. R. J. Bobber 1988 *Underwater Electroacoustic Measurements*. Los Altos, CA: Peninsula Publishing.
11. B. K. Novikov, O. V. Rudenko, and V. I. Timoshenko 1987 *Nonlinear Underwater Acoustics*. New York, Acoustical Society of America.
12. D. B. Keele Jr., 1975 *Journal of the Audio Engineering Society* (Abstracts) **23**, 492 (preprint 1038, presented at the 51st Convention of the Audio Engineering Society). What's so sacred about exponential horns.
13. G. W. Stewart and R. B. Lindsay 1940 *Acoustics*, 212. Pricenton, NJ: Van Nostrand.
14. L. L. Beranek 1996 *Acoustics*. New York: Acoustical Society of America/American Institute of Physics.
15. P. M. Morse 1976 *Vibration and Sound*, 265–288. New York: Acoustical Society of America/ American Institute of Physics.
16. L. E. Kinsler 1982 *Fundamentals of Acoustics*, third edition. New York: John Wiley & Sons.
17. A. G. Webster 1919 *Proceedings of the National Academy of Science* **5**, 275–282. Acoustical impedance and the theory of horns and of the phonograph.
18. A. H. Benade 1988 *Journal of the Acoustical Society of America* **83**, 1764–1769. Equivalent circuits for conical waveguides.
19. R. L. Clark, R. Fuller, and Al. Wicks 1991 *Journal of the Acoustical Society of America* **90**, 346–357. Characterization of multiple piezoelectric actuators for structural excitation.
20. B. T. Wang 1996 *Journal of the Acoustical Society of America* **99**, 2975–2984. Optimal placement of microphones and piezoelectric transducer actuators for far-field sound radiation control.